

Review

Optical Terahertz Sources Based on Difference Frequency Generation in Nonlinear Crystals

Yang Liu ^{1,2,3,*}, Kai Zhong ⁴ , Aiqiang Wang ^{1,2}, Mengchen Zhou ^{1,2}, Shanchuang Li ^{1,2}, Lu Gao ⁵ and Ze Zhang ^{1,2,*}

- ¹ Qilu Aerospace Information Research Institute, Jinan 250100, China; wangaq01@aircas.ac.cn (A.W.); zhoumc@aircas.ac.cn (M.Z.); lishanc@aircas.ac.cn (S.L.)
- ² Aerospace Information Research Institute, Chinese Academy of Sciences, Beijing 100094, China
- ³ Science and Technology on Solid-State Laser Laboratory, Beijing 100015, China
- ⁴ Key Laboratory of Optoelectronics Information Technology (Ministry of Education), School of Precision Instruments and Opto-Electronics Engineering, Tianjin University, Tianjin 300072, China; zhongkai@tju.edu.cn
- ⁵ School of Science, China University of Geosciences, Beijing 100083, China; gaolu@cugb.edu.cn
- * Correspondence: liuyang01@aircas.ac.cn (Y.L.); zhangze@aircas.ac.cn (Z.Z.)

Abstract: Terahertz (THz) sources, ranging from 0.1 THz to 10 THz, between microwaves and infrared waves, have important applications in spectral detection, medical imaging, communication, etc. Difference frequency generation (DFG) is an effective method for generating terahertz with the characteristics of low cost, simple structure, widely tunable range, no threshold, and room-temperature operation. This paper reviews various optical terahertz sources of difference frequency generation based on nonlinear crystals, including DFG with inorganic crystals, DFG with organic crystals, DFG with quasi-phase-matching (QPM) crystals, DFG in waveguides, cavity-enhanced DFG, and cascaded DFG. Their recent advances, as well as their advantages and disadvantages, are fully present and discussed. This review is expected to provide a comprehensive reference for researchers in this field and a quick understanding of optical THz sources of difference frequency generation with nonlinear crystals.

Keywords: terahertz wave; difference frequency generation; DGF crystal; inorganic crystal; organic crystal; QPM crystal



Citation: Liu, Y.; Zhong, K.; Wang, A.; Zhou, M.; Li, S.; Gao, L.; Zhang, Z. Optical Terahertz Sources Based on Difference Frequency Generation in Nonlinear Crystals. *Crystals* **2022**, *12*, 936. <https://doi.org/10.3390/cryst12070936>

Academic Editor: Martin Dressel

Received: 9 June 2022

Accepted: 29 June 2022

Published: 1 July 2022

Publisher's Note: MDPI stays neutral with regard to jurisdictional claims in published maps and institutional affiliations.



Copyright: © 2022 by the authors. Licensee MDPI, Basel, Switzerland. This article is an open access article distributed under the terms and conditions of the Creative Commons Attribution (CC BY) license (<https://creativecommons.org/licenses/by/4.0/>).

1. Introduction

The terahertz (THz) “gap” corresponding to the frequency range of 0.1–10 THz (3 mm to 30 μm in wavelength), between microwaves and infrared (IR) waves, was the last electromagnetic band to be exploited and utilized. Since the 1960s, optical methods to obtain THz radiation have also achieved breakthrough progress [1,2], and their related applications have become gradually commercialized and marketed with the leap in development of laser and material science. Due to the unique properties of low energy, water absorption, penetration, and fingerprint characteristics, terahertz waves have good prospects in high-resolution spectroscopy, radar, imaging, communication, and nondestructive inspection [3–7].

At present, the methods of terahertz generation are divided into electronic and photonic technology. The electronic methods usually generate relatively low-frequency terahertz radiation (below 1 THz), such as gyrotrons and Gunn diodes [8,9]. Although a free-electron laser with large size and high cost can realize broadband terahertz wave, it is difficult to apply widely [10,11]. In contrast, photonic technology can achieve a wider frequency range of terahertz radiation with a smaller and less expensive structure. Optical terahertz sources mainly include the optically pumped gas terahertz laser, the quantum cascade laser, photoconduction, and nonlinear optical frequency conversion. The optically pumped gas terahertz laser suffers from complicated operation and is bulky; thus, the size

needs to be simplified and the efficiency and stability need to be improved for applications [12–14]. The quantum cascade laser is an important breakthrough for miniaturizing terahertz sources with the advantages of small size, low energy consumption, and easy integration, but it can only work in a low-temperature environment [15]. Moreover, terahertz waves generated by photoconductive antennas have higher power, but their frequencies are usually low [16–18].

The terahertz source of difference frequency generation (DFG) is a typical representative of nonlinear optical frequency conversion. There is no threshold in the DFG process, along with low cost, simple structure, and room-temperature operation. In addition, changing the pump wavelength or nonlinear crystal can achieve a widely tunable and narrow-linewidth terahertz wave output. In this review, the recent advances and developments of various DFG terahertz sources are fully presented, including DFG with inorganic crystals, DFG with organic crystals, DFG with quasi-phase-matching (QPM) crystals, DFG in waveguides, cavity-enhanced DFG, and cascaded DFG.

2. Theory of Difference Frequency Generation

DFG makes use of second-order ($\chi^{(2)}$) nonlinear materials for achieving THz waves under the condition of phase matching (PM). Two laser beams with similar frequencies ω_1 and ω_2 are used to generate coherent THz radiation (ω_T), whose frequency is the difference ($\omega_1 - \omega_2 = \omega_T$) between the frequencies of the two lasers through a nonlinear medium. Ignoring the absorptions and reflections of the crystal, the DFG THz intensity in the small-signal approximation based on the plane-wave model can be expressed as

$$I_T = \frac{1}{2} \left(\frac{\mu_0}{\varepsilon_0} \right)^{1/2} \frac{\omega_T^2 (2d)^2 L^2}{n_1 n_2 n_T c^2} I_1 I_2 \times \frac{\sin^2 \left(\frac{1}{2} \Delta k L \right)}{\left(\frac{1}{2} \Delta k L \right)^2}, \quad (1)$$

where I_T is the generated THz intensity, I_1 and I_2 are the incident laser intensity, ε_0 is the permittivity of free space, μ_0 is the magnetoconductivity, d is the efficient nonlinear coefficient, L is the crystal length, n_1 , n_2 , and n_T are the refractive indices of incident laser and THz frequencies, and Δk is the phase mismatch factor. The PM in the DFG process is $\Delta k = k_1 - k_2 - k_T = 0$. Figure 1 shows a schematic diagram of collinear PM and noncollinear PM. The condition of collinear PM can be written as

$$\Delta k = \frac{n_1 \omega_1}{c} - \frac{n_2 \omega_2}{c} - \frac{n_T \omega_T}{c}, \quad (2)$$

while the PM condition ($\Delta k = 0$) of noncollinear DFG is as follows [19]:

$$\sin \frac{\theta}{2} = \left[\frac{n_3 (\omega_T)^2 - (n_1 \omega_1 - n_2 \omega_2)^2}{4 n_1 n_2 \omega_1 \omega_2} \right]^{1/2}, \quad (3)$$

$$\cos \varphi = \left[1 + 2 \frac{\omega_2}{\omega_T} \sin^2 \left(\frac{\theta}{2} \right) \right] \times \left[1 + 4 \frac{\omega_1 \omega_2}{(\omega_T)^2} \sin^2 \left(\frac{\theta}{2} \right) \right]^{-1/2}, \quad (4)$$

where θ is the angle between k_1 and k_2 , and φ is the angle between k_T and k_1 .

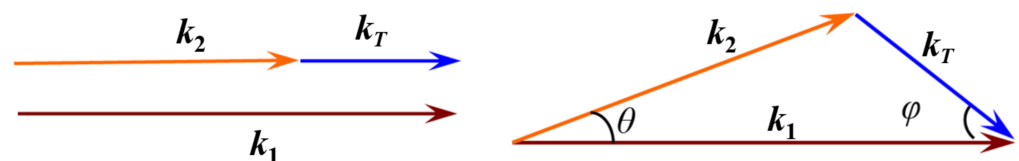


Figure 1. Schematic diagram of collinear PM and noncollinear PM.

Inorganic crystals commonly utilize a birefringence effect or residual radiation band with dispersion compensation to achieve PM. According to the birefringence characteristics

of anisotropic crystals, phase matching can be achieved by selecting appropriate k -vectors and polarization directions (o- or e-polarized) in the collinear interaction, such as GaSe, ZnGeP2 (ZGP), and LiNbO₃ crystals. Some isotropic nonlinear materials lack birefringence such as GaAs, GaP, and ZnTe, which can use a residual radiation band with abnormal dispersion to satisfy noncollinear PM. Figure 2 shows an example of the collinear PM angle with GaSe and the noncollinear PM angle with GaAs. The wavelengths of the pump lasers were $\lambda_1 = 1.95 \mu\text{m}$ for both, while λ_2 ranged from $1.957 \mu\text{m}$ to $2.020 \mu\text{m}$. Theoretically, a THz wave output of $0.55\text{--}5.33 \text{ THz}$ can be generated.

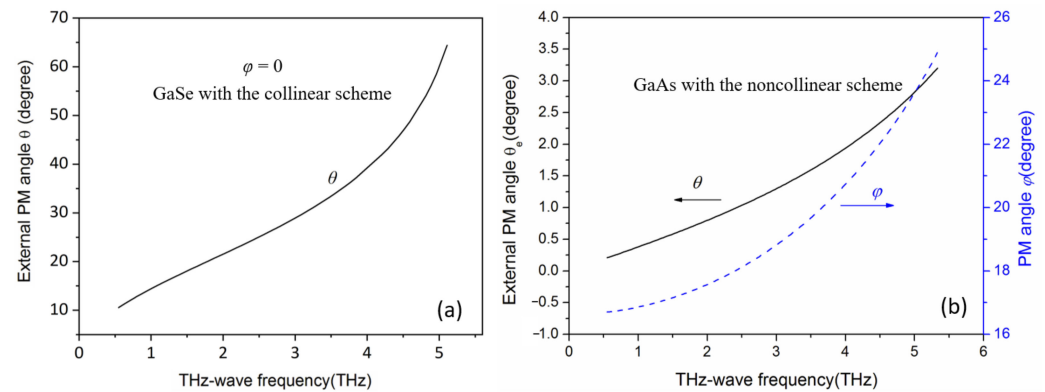


Figure 2. (a) The collinear phase matching angle with GaSe; (b) the noncollinear phase matching angle with GaAs.

According to the Manley–Rowe relation, a pump photon is divided into an idle photon and a terahertz photon in the process of DFG. The variation of power rate between three waves is expressed as

$$\frac{\Delta P_{\omega_T}}{\omega_T} = \frac{\Delta P_{\omega_2}}{\omega_2} = -\frac{\Delta P_{\omega_1}}{\omega_1}, \quad (5)$$

where ΔP is the power rate variation with a frequency of ω . The maximum quantum efficiency in the DFG process is determined by

$$\eta_{max} = \frac{\omega_T}{\omega_1} = \frac{\lambda_1}{\lambda_T}, \quad (6)$$

where η_{max} is the maximum quantum efficiency. A longer pump wavelength has a higher power conversion efficiency when the terahertz wavelength is constant.

3. DFG Terahertz Sources with Inorganic Crystals

In addition to the quantum defect and the k -vector mismatch, the nonlinear coefficient and absorption coefficient of crystals also have a great influence on the DFG efficiency. Table 1 shows main pump bands of common inorganic crystals with various operating modes. The GaAs crystal with a considerable nonlinear coefficient has strong two-photon absorption in the near-infrared band [20,21]. Generally, adopting mid-infrared lasers of about $10 \mu\text{m}$ generated by a bulky and complicated CO₂ laser can achieve a higher output power of terahertz in the DGF process. In 2011, Lu et al. reported that the average power of terahertz waves was about $10 \mu\text{W}$, and the frequency range was $0.11\text{--}4.15 \text{ THz}$ pumped with a nanosecond pulse and low-repetition frequency [22]. When a picosecond laser was used as the pump source, the peak power of THz waves could reach 2 MW [23]. In comparison, the absorption coefficient of the GaSe crystal is relatively smaller than various DFG crystals [24,25]. Flexible pump wavelengths have been employed to obtain the THz output. Leitenstorfer and Huber carried out collinear and noncollinear DFG with femtosecond pulses, where THz peak powers of 100 MW/cm were achieved [26]. High-repetition operation is required if some terahertz applications need to increase the sampling rate. Ding et al. reported a terahertz source with a frequency difference of 0.914 THz and

average power of 260 μ W using a high-repetition-frequency CO₂ laser [27]. Later, they realized terahertz output pumped by a compact Q-switched Nd:YLF dual-frequency laser at 1047 and 1053 nm, while the timing jitter of pulses was usually uncontrolled [28,29]. Recently, we proposed a flexible method to adjust the time interval and power ratio of dual-wavelength laser for THz generation based on the end-pumping configuration with two coaxially arranged Nd:YLF crystals [30], as shown in Figure 3, which could solve the problem of the timing jitter. Moreover, a tunable 2 μ m optical parametric oscillator (OPO) for generating THz waves with a GaSe crystal was also investigated [31,32]. Degenerate 2 μ m lasers with a short pulse duration are good for enhancing the DFG efficiency, as they are efficient, simple, and widely tunable. A microwatt output power and a range of 0.41–3.71 THz were enough to apply to imaging and spectroscopy. The tunable range was extended to 0.24–3.78 THz when the KTP was replaced with a type-II QPM PPLN crystal [33].

Table 1. Main pump bands of common inorganic crystals with various operating modes.

Operating Mode	Pump Wavelength	Inorganic Crystals
Femtosecond pulse	1–1.5 μ m	GaSe
Picosecond pulse	1 μ m	LiNbO ₃
	10 μ m	GaAs
Nanosecond laser	1 μ m	GaSe, ZGP, GaP, LiNbO ₃
	1.3–1.5 μ m	GaSe, LiNbO ₃
	2 μ m	GaSe
Continuous wave	10 μ m	GaSe, GaAs
	1 μ m	GaP

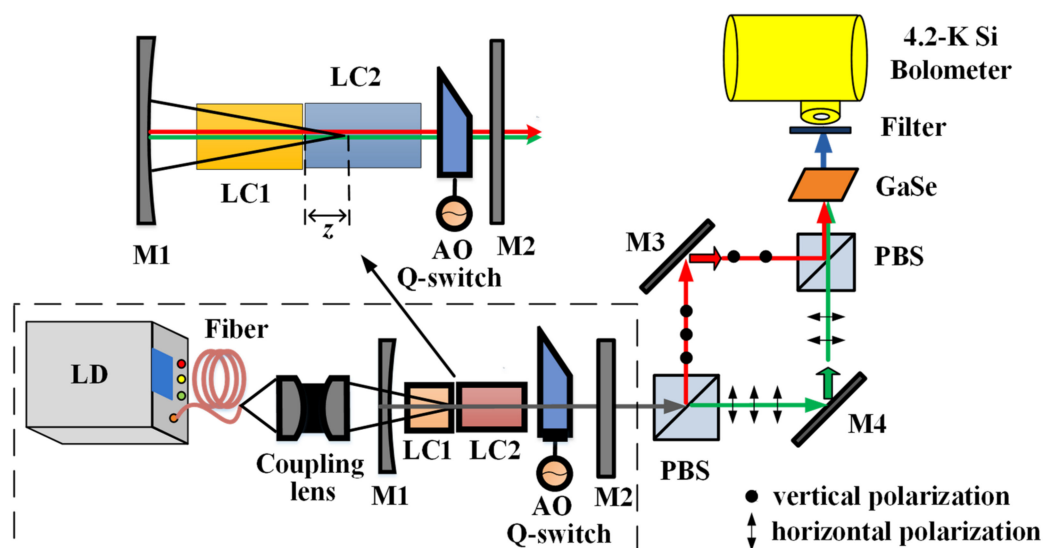


Figure 3. Experimental layout of the compact THz source based on a coaxial pumping dual-frequency solid-state laser [30]. LC1 and LC2 are two coaxially arranged Nd:YLF crystals to solve the problem of the timing jitter. M1–M2: cavity mirrors. M3–M4: reflective mirrors. AO Q-switch: acousto-optic Q-switch. LD: laser diode. PBS: polarizing beam splitter.

For LiNbO₃ crystals, serious absorption in the THz range limits the output power and tunability. An energy of about 1.58 nJ was achieved by using a 1 μ m dual-wavelength pump laser at a low repetition frequency [34]. A ZnGeP₂ (ZGP) crystal with a large nonlinear coefficient and high damage threshold is commonly used for DFG with a THz output [35,36]. However, it has a higher absorption coefficient around 1 μ m, restricting power scaling [37]. Creeden et al. realized an average power of 2 mW by using two all-fiber laser amplifiers, which is among the highest power recorded for DFG THz sources [38]. The GaP crystal has

a very low two-photon absorption in the near-infrared region. A 1 μm dual-wavelength laser is usually used to improve the DFG efficiency. An average power of 27 nW at 6 kHz and a peak power of 40 W at the repetition frequency of 10 Hz were reported [39,40]. Furthermore, tunable THz sources were also achieved using GaP crystals [41–43].

In general, inorganic crystals have extremely large absorption coefficients above 5 THz limited by their lateral lattice vibrations. Therefore, the tuning range of THz sources is usually in the range of 0.1–5 THz, which is hard to cover the entire THz band.

4. DFG Terahertz Sources with Organic Crystals

Organic crystals have smaller absorption coefficients in the high-frequency THz band. Moreover, their dispersion characteristics are close and stable between the infrared band and the THz band, such that the type 0 collinear phase matching with loose condition can be met. On the basis of the D- π -A structure, an organic crystal with a larger nonlinear coefficient can easily achieve higher conversion efficiency. The DAST crystal is currently the most mature organic crystal, which has been proven to be an ideal nonlinear optical material in THz generation [44]. In 1999, Riken's group used a DAST crystal pumped by a 800 nm dual-wavelength Ti-sapphire laser to achieve difference frequency generation with a THz wave output [45]. The DAST crystal had a greater coherence length in the ultrabroadband THz frequency range when the wavelength of the pump laser was 1.3–1.5 μm . In 2004, Taniuchi et al. reported that the tuning range of a DFG terahertz source was extended to 2–30 THz with KTP-OPO by generating tunable dual-wavelength lasers around 1.3 μm [46]. Figure 4 shows a typical ultra-broadband tunable THz configuration with organic crystal. A double-pass OPO based on a reflective structure was carried out for improving the pump efficiency in 2007 [47].

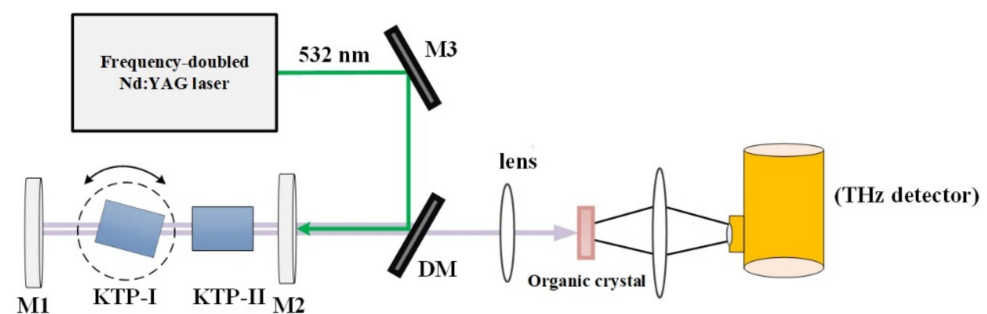


Figure 4. Typical ultra-broadband tunable THz configuration with organic crystal pumped by a double-pass OPO. M1–M2: OPO mirrors. M3: reflective mirror. DM: dichroic mirror.

Furthermore, a variety of high-performance dual-wavelength lasers and optimizing methods have been applied to DFG THz sources based on DAST crystals for high-efficiency terahertz output, including KTP-OPO intracavity pumping [48], CW dual-wavelength fiber laser [49], BBO-OPO [50], PPLN optical parametric generation (OPG) with seed injection [51], BBO-OPG [52], and dual-wavelength Nd:YAG laser [53]. Table 2 shows the performance of DFG THz radiation sources based on DAST crystals. In 2012, Uchida et al. used the annealing method to increase the damage threshold of DAST crystals to 1.1 GW/cm², which could effectively improve the output energy of THz waves [54]. Liu et al. specifically analyzed the optimal pumping conditions in various dual-wavelength pump sources [55]. He et al. realized a THz frequency-domain spectroscopy system based on an ultra-broadband tunable THz radiation source with a DAST crystal, which could be directly applied to material spectroscopy measurements [56].

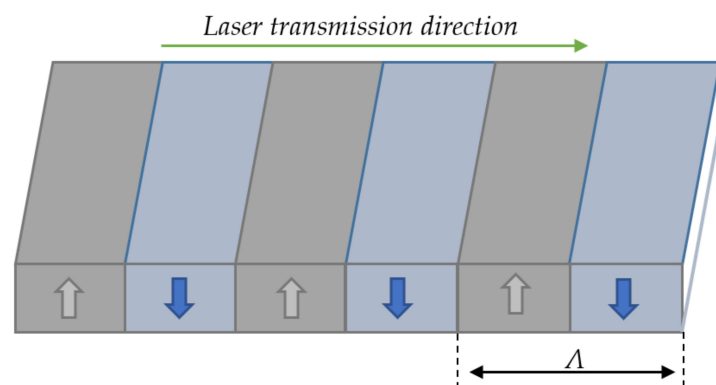
Table 2. Performance of DFG THz radiation sources based on DAST crystal [45–53].

Year	Dual-Wavelength Lasers	Pump Intensity	THz Output	THz Wavelength
1991	Ti-sapphire laser	600 μJ	80 fJ	1.4 THz
2004	PPLN-OPO	0.75 mJ	180 nJ	2–30 THz
2007	KTP-OPO	21 mJ	μJ level	1–30 THz
2008	KTP-OPO intracavity pumping	168 MW/cm^2	0.4 mW	2–4 THz
2011	CW fiber laser	0.8 W	-	0.5–2 THz
2012	BBO-OPO	2.5 mJ	-	1–30 THz
2015	Seed injection PPLN-OPG	80 μJ	14.7 nJ	1.5–27 THz
2017	BBO-OPG	0.44 mJ	80 pJ	0.3–4 THz
2017	1.3- μm Nd:YAG laser	1.68 MW/cm^2	0.58 μW	3.28 THz

With respect to DAST crystals, all kinds of DAST homologs including DSTMS, DASC, and other crystals have been successfully grown by replacing the anion group [57–59]. In 2014, Liu et al. reported an ultra-broadband tunable THz source with a tuning range of 0.88–19.27 THz from a DSTMS crystal [60]. It is worth noting that large organic crystals are difficult to grow, which limits their application. Furthermore, the output spectrum of THz waves based on DAST crystals and their homologs has a dip around 1.1 THz due to the intrinsic absorption characteristics [61]. Optimizing the crystal structure according to the needs with a short growth cycle can solve the problem of intrinsic absorption modes. Various types of organic crystals have been developed, such as OH1, BNA, HMQ-T, and HMQ-TMS crystals [62–66].

5. DFG Terahertz Sources with Quasi-Phase-Matching Crystals

Quasi-phase-matching technique is a flexible approach to meet PM without utilizing birefringence, which can use the entire transmission range and the largest nonlinear coefficient of the crystal. Thus, the nonlinear conversion efficiency is high, and the space walk-off effect can be avoided. The PM condition of the QPM crystal becomes $\Delta k = k_1 - k_2 - k_T - k_\Lambda = 0$, $k_\Lambda = 2\pi m/\Lambda$, where Λ is the QPM period, and m is the QPM order. The k_Λ designed into the required form is used to compensate for phase mismatch. Figure 5 shows schematic diagram of the principle of quasi-phase matching.

**Figure 5.** Schematic diagram of the principle of quasi-phase matching. Arrows indicate polarized direction.

The methods for achieving QPM mainly include periodical poling (PP) [67], stacking crystal plates with periodical rotations of 180° [68], and orientation-patterned (OP) epitaxial growth [69]. Among the quasi-phase matching devices, the periodically polarized lithium niobate (PPLN) crystal is the most commonly applied to THz wave generation. In 2002, Sasaki et al. reported the THz wave surface radiation using the slant-stripe PPLN crystal [70]. Later, they achieved a 11.4 nW DFG terahertz source with a peak power of 0.1 mW pumped by a 1.5 μm dual-wavelength pulse laser (1 MHz, 100 ps) [71]. An average power of about 2 mW was achieved using the 1 μm CW dual-wavelength laser [72]. More-

over, forward or backward DFG for terahertz generation could also be realized by using a multi-grating PPLN crystal [73]. Table 3 shows the performance of DFG THz radiation sources based on QPM crystals.

Adopting orientation-patterned epitaxial growth or the diffusion bonding technique based on QPM can solve the problem of isotropic crystals (such as GaAs and GaP) struggling to meet phase matching during the DGF process [74]. This gives full play to the advantages of large nonlinear coefficient and small THz absorption, effectively improving the generation efficiency of terahertz waves. Periodically inverted GaP has low absorption in the near-IR range, which enhances the conversion efficiency for terahertz generation [75]. In 2011, Petersen et al. achieved terahertz output with an average power of 339 μ W and peak power of 212 mW pumped by a 1.5 μ m pulse laser with a repetition frequency of 20 kHz [76]. Jiang et al. reported terahertz output with a peak power of 3.77 kW using a 1 μ m pump laser at a low repetition frequency [77]. For QPM-GaAs, a DFG terahertz source with efficient optical-to-THz output pumped by a 2 μ m picosecond dual-wavelength laser could be realized [78,79]. The maximum average output power of a tunable continuous-wave (CW) THz DFG source was beyond 1 mW when using QPM-GaAs [80].

Table 3. Performance of DFG THz radiation sources based on QPM crystals [71,72,76,79,80].

QPM Crystal	Dual-Wavelength Lasers	THz Output	THz Wavelength
PPLN	1.5 μ m laser (1 MHz, 100 ps)	11.4 nW	1.5–1.8 THz
PPLN	1 μ m CW laser	2 mW	1.9 THz
QPM GaP	1.5 μ m pulse laser (20 KHz)	339 μ W	1.5 THz
QPM-GaAs	2 μ m laser (50 MHz, 7 ps)	1 mW	2.8 THz
OP-GaAs	2 μ m CW laser	2 mW	1–4.5 THz

6. DFG Terahertz Sources with Waveguides

Compared to bulk nonlinear crystals, waveguide structures provide better mode confinement to enhance the output intensity and DFG efficiency. Using waveguide structures with different dispersion can achieve various phase matching properties between different modes of light waves. Figure 6 shows a structure diagram of a ridge waveguide, which was used as an example to calculate the effective refractive index for phase matching, where w_r is the ridge width of the ridge waveguide, h is the ridge height, t and h are the thickness of the central coating and both sides, b is the thickness of the plate part, and the thickness of the waveguide base is infinite. Furthermore, n_a , n_c , n_r , and n_s represent the refractive index of air, surface coating, waveguide material, and substrate, respectively, while n_1 and n_2 are the effective refractive index of regions I and II. Here, the effective refractive index of a ridge waveguide was analyzed, according to the method proposed by Tyszkiewicz [81].

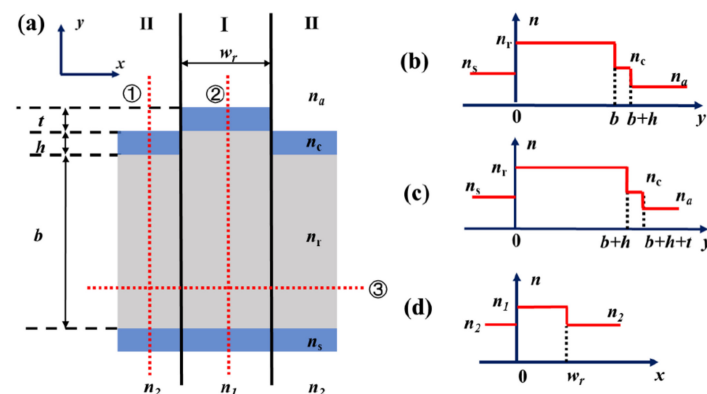


Figure 6. (a) Structure diagram of ridge waveguide; (b) refraction index profile of the red dotted line 1; (c) refraction index profile of the red dotted line 2; (d) refraction index profile of the red dotted line 3.

Both sides of the waveguide are assumed to be infinitely long. For the central region I, the dispersion equation is

$$\frac{2\pi}{\lambda_0}(b+h+t)\sqrt{n_r^2-n_1^2} = \tan^{-1}\left[\left(\frac{n_r}{n_s}\right)^{2\rho}\sqrt{\frac{n_1^2-n_s^2}{n_r^2-n_1^2}}\right] + \tan^{-1}\left[\frac{\xi\psi\cosh\varphi - \sinh\varphi}{\psi\cosh\varphi + \sinh\varphi}\right], \quad (7)$$

where λ_0 is the wavelength in vacuum, $\rho = 0$ is the TE mode, and $\rho = 1$ is the TM mode. ξ , ψ , and φ can be expressed as

$$\xi = \left(\frac{n_r}{n_c}\right)^{2\rho}\sqrt{\frac{n_1^2-n_c^2}{n_r^2-n_1^2}}, \quad \psi = \left(\frac{n_c}{n_s}\right)^{2\rho}\sqrt{\frac{n_1^2-n_a^2}{n_1^2-n_c^2}}, \quad \varphi = \frac{2\pi}{\lambda_0}t\sqrt{n_1^2-n_c^2}, \quad (8)$$

and the above calculation process is based on the fundamental mode of TE and TM. For the region of both sides II, the dispersion equation is

$$\frac{2\pi}{\lambda_0}(b+h)\sqrt{n_r^2-n_2^2} = \tan^{-1}\left[\left(\frac{n_r}{n_s}\right)^{2\rho}\sqrt{\frac{n_1^2-n_s^2}{n_r^2-n_2^2}}\right] + \tan^{-1}\left[\frac{\xi'\psi'\cosh\varphi' - \sinh\varphi'}{\psi'\cosh\varphi' + \sinh\varphi'}\right], \quad (9)$$

where ξ' , ψ' , and φ' can be expressed as

$$\xi' = \left(\frac{n_r}{n_c}\right)^{2\rho}\sqrt{\frac{n_2^2-n_c^2}{n_r^2-n_2^2}}, \quad \psi' = \left(\frac{n_c}{n_s}\right)^{2\rho}\sqrt{\frac{n_2^2-n_a^2}{n_2^2-n_c^2}}, \quad \varphi' = \frac{2\pi}{\lambda_0}h\sqrt{n_2^2-n_c^2}, \quad (10)$$

and the effective refractive index n_3 satisfies the following equation:

$$\frac{2\pi}{\lambda_0}(w_r)\sqrt{n_1^2-n_2^2} = 2\tan^{-1}\left[\left(\frac{n_1}{n_2}\right)^{2\rho}\sqrt{\frac{(n_3^2-n_2^2)}{(n_1^2-n_2^2)}}\right], \quad (11)$$

where n_3 is the effective refractive index of the whole waveguide structure.

Thompson and Coleman first achieved THz output with nanowatt power from a planar GaAs waveguide using a CO₂ laser [82]. Later, various DFG THz sources based on GaAs waveguides were investigated [83,84]. Table 4 shows the performance of DFG THz radiation sources based on various waveguides. Using a 2 μm dual-wavelength laser and GaAs planar waveguides, the average power of terahertz waves at 2 THz could reach 1 μW [85]. By flexibly designing the waveguide structure of GaP, a high-power THz output with a wide tuning range could be realized [86–88]. When LiNbO₃ crystal was used as the waveguide medium, the output power of the THz wave was about 0.5 μW , and the frequency range covered 0.97–7.5 THz, pumped by a 1.5 μm CW dual-wavelength laser [89]. Suizu et al. reported that an average power of 400 pW and peak power of 4 μW were obtained using a PPLN waveguide [90].

A silicon waveguide was studied by strain-induced second-order nonlinearity, demonstrating promising potential for high-power THz generation [91]. Recently, Schulz et al. reported that the output power of terahertz waves was 10 μW with a tunable range of 1–10 THz based on an integrated nonlinear waveguide of silicon [92]. A metallic–dielectric hybrid (MDH) waveguide for THz parametric interactions was theoretically analyzed by Ding [93]. The strength of terahertz parametric converter was significantly enhanced by reducing the modal indices and eliminating the diffraction in forward or backward generation. Liu et al. proposed a high-power terahertz source with high brightness using nonlinear optical crystal fiber, which consisted of a GaAs core with periodical inversion [94]. Cherchi et al. thoroughly compared dielectric waveguides composed of zincblende semiconductors, exploiting the optical nonlinearity for guiding terahertz generation [95]. Recently, we theoretically investigated a category of ridge waveguides composed of GaAs and SiN in different sizes for efficient terahertz generation [96]. The output power and conversion efficiency based on integrated hybrid waveguides were much higher than

those using bulk or micro-structured GaAs crystals, revealing their potential for on-chip terahertz systems.

Table 4. Performances of DFG THz radiation sources based on various waveguides [85,88–90,92].

Waveguide Type	Dual-Wavelength Lasers	THz Output	THz Wavelength
GaAs waveguide	2 μm laser (50 MHz, 7 ps)	1 μW	2 THz
GaP waveguide	OPO with 0.92–1.5 μm	56 pJ	0.48–4.3 THz
LiNbO ₃ waveguide	1.5 μm CW laser	0.5 μW	0.97–7.5 THz
PPLN waveguide	1.5 μm laser (1 MHz, 100 ps)	400 pW	1.48 THz
silicon waveguide	1.5 μm CW laser	10 μW	1–10 THz

In addition to the abovementioned DFG materials, the DFG medium based on quantum wells could also realize frequency conversion using the quantum confinement effect. A quantum well structure with the designed energy level based on GaAs/AlAs was used to produce THz waves [97–99].

7. Cavity-Enhanced DFG and Cascaded DFG

Although various DFG materials have been extended to increase the DFG efficiency, the THz conversion efficiency of a single-pass nonlinear crystal is usually low due to the limitation of pump intensity. Recycling the laser pulses is a practical approach to obtain high-power THz output through an external enhancement cavity. Figure 7 shows a typical external enhancement cavity with a bow-tie configuration. A piezoelectric transducer (PZT) is used to fine-tune the cavity length. The enhancement factor can be maximized by providing small cavity round trip losses (Δ) with the optimized enhancement cavity. The maximum enhancement factor A in the CW case is written as follows [100]:

$$A = \frac{1 - R}{\left[1 - \sqrt{R(1 - \Delta)}\right]^2 + 4\sqrt{R(1 - \Delta)} \sin^2\left(\frac{\delta}{2}\right)}, \quad (12)$$

where R is the cavity reflectivity, and δ is the difference of phase between two consecutive round trips.

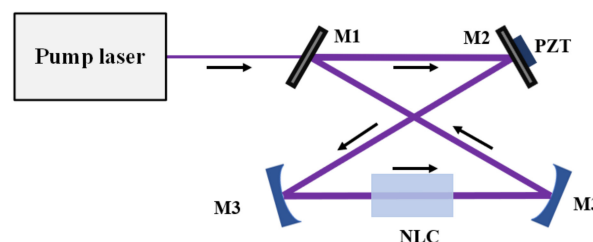


Figure 7. Typical external enhancement cavity with bow-tie configuration. M1–M2: cavity mirrors. NLC: nonlinear crystal. PZT: piezoelectric transducer.

Steady-state lasers with external cavity-enhanced nonlinear frequency conversions were investigated in CW, nanosecond, and femtosecond operation [101–103]. In 2010, Petersen et al. reported an enhanced terahertz generation with a resonant external cavity, which realized a sevenfold enhancement compared with a single-pass orientation [104]. Later, they greatly improved the enhancement factor by 250 times using QPM GaP [76]. In terms of narrow linewidth, Paul et al. proposed a single-frequency terahertz source exceeding 100 μW using an external enhancement cavity for DFG [105].

Due to the barrier of inherent quantum defects, the conversion ratio between near-IR and THz ranges was also restricted (see Equation (6)). The cascade DFG generates multiple terahertz photons from the depletion of a single pump photon, which provides a feasible approach to break the constraint of the Manley–Rowe relation. The basic concept of cascaded DFG terahertz radiation is shown in Figure 8. A terahertz photon with frequency

of ω_T is generated by the interaction between a high-frequency pump photon with a frequency of ω_m and a low-frequency pump photon with a frequency of ω_{m+1} , while the low-frequency pump photon is amplified. If the gain is high in the DFG process, the amplified pump photon as a new high-frequency pump photon interacts with the terahertz wave to generate a new low-frequency pump photon with a frequency of ω_{m+2} . Meanwhile, the THz photon with a frequency of ω_T is amplified. The repeated conversion of energy between high-frequency pump light and low-frequency light continuously generates a series of THz photons under the condition of phase matching.



Figure 8. Schematic diagram of cascaded DFG terahertz radiation.

A birefringent crystal with anisotropy cannot satisfy the cascade conditions limited by polarization and parameters. Isotropic crystals such as GaP, GaAs, and ZnTe are usually applicable for the cascade DFG. In 2004, Cronin-Golomb first predicted cascaded DFG for enhanced THz generation from ZnTe using a 800 nm laser [106]. In 2008, Schaar et al. used a GaAs crystal based on quasi-phase matching technology to generate terahertz waves and detected both Stokes light and anti-Stokes light in the experiment, confirming the cascade process [107]. Later, the dynamic process of cascaded DFG in QPM crystals and isotropic crystals for optimal designing parameters was theoretically analyzed [108,109]. In 2016, Ravi et al. proposed a high-energy terahertz generation technology based on spectrally cascaded optical parametric amplification from PPLN under low-temperature cooling cycles [110]. The light waves with different order were formed by the repeated energy conversion from the first-order high-frequency pump light to the low-frequency light in the cascade process. Therefore, cascading DFG for terahertz output can be further enhanced by increasing the order and improving the period variation of the crystal.

8. Conclusions

This paper provided a review of optical terahertz sources of difference frequency generation, including DFG with inorganic crystals, DFG with organic crystals, DFG with quasi-phase-matching crystals, DFG in waveguides, cavity-enhanced DFG, and cascaded DFG. Various kinds of operating modes involved in Q-switching, CW, single frequency, or tunability were covered. The terahertz radiation generated by the DFG method can meet the needs of many applications, such as spectroscopy and imaging. Optimizing the DFG THz source based on nonlinear crystals is of great significance to the development and application of terahertz technology. This review is expected to provide a comprehensive reference for researchers and help to push the progress of optical THz sources based on difference frequency generation with nonlinear crystals.

Funding: This research was funded by the National Natural Science Foundation of China (Grant No. 62105341, Grant No. 12074350), the Natural Science Foundation of Shandong Province (Grant No. ZR2021QF126), and the Science and Technology on Solid-State Laser Laboratory Stability Support Project.

Institutional Review Board Statement: Not applicable.

Informed Consent Statement: Not applicable.

Data Availability Statement: Not applicable.

Acknowledgments: The authors thank Longhuang Tang for his help with the technical support.

Conflicts of Interest: The authors declare no conflict of interest.

References

1. Akhmanov, S.A.; Khokhlov, R.V. Concerning one possibility of amplification of light waves. *Sov. Phys. JETP* **1963**, *16*, 252–257.
2. Yajima, T.; Inoue, K. Submillimeter-wave generation by optical difference-frequency mixing of ruby R1 and R2 laser lines. *Phys. Lett. A* **1968**, *26*, 281–282. [[CrossRef](#)]
3. Loeffler, T.; Siebert, K.; Czasch, S.; Bauer, T.; Roskos, H.G. Visualization and classification in biomedical terahertz pulsed imaging. *Phys. Med. Biol.* **2002**, *47*, 3847. [[CrossRef](#)]
4. Hindle, F.; Cuisset, A.; Bocquet, R.; Mouret, G. Continuous-wave terahertz by photomixing: Applications to gas phase pollutant detection and quantification. *Comp. Rend. Phys.* **2008**, *9*, 262–275. [[CrossRef](#)]
5. Zhan, H.; Zhao, K.; Bao, R.; Xiao, L. Monitoring PM2.5 in the atmosphere by using terahertz time-domain spectroscopy. *J. Infrared Millim. Terahertz Waves* **2016**, *37*, 929–938. [[CrossRef](#)]
6. Iwaszczuk, K.; Heiselberg, H.; Jepsen, P.U. Terahertz radar cross section measurements. *Opt. Express* **2010**, *18*, 26399–26408. [[CrossRef](#)] [[PubMed](#)]
7. Zhong, K.; Shi, W.; Xu, D.G.; Liu, P.X.; Wang, Y.Y.; Mei, J.L.; Yan, C.; Fu, S.J.; Yao, J.Q. Optically pumped terahertz sources. *Sci. China Technol. Sci.* **2017**, *60*, 1801–1818. [[CrossRef](#)]
8. Lewis, R.A. A review of terahertz sources. *J. Phys. D Appl. Phys.* **2014**, *47*, 374001. [[CrossRef](#)]
9. Federici, J.; Moeller, L. Review of terahertz and subterahertz wireless communications. *J. Appl. Phys.* **2010**, *107*, 111101. [[CrossRef](#)]
10. Knyazev, B.A.; Kulipanov, G.N.; Vinokurov, N.A. Novosibirsk terahertz free electron laser: Instrumentation development and experimental achievements. *Meas. Sci. Technol.* **2010**, *21*, 54017. [[CrossRef](#)]
11. Tan, P.; Huang, J.; Liu, K.F.; Xiong, Y.Q.; Fan, M.W. Terahertz radiation sources based on free electron lasers and their applications. *Sci. China Inform. Sci.* **2012**, *55*, 1–15. [[CrossRef](#)]
12. Shumyatsky, P.; Alfano, R.R. Terahertz sources. *J. Biomed. Opt.* **2001**, *16*, 33001. [[CrossRef](#)]
13. Dodel, G. On the history of far-infrared (FIR) gas lasers: Thirty-five years of research and application. *Infrared Phys. Technol.* **1999**, *40*, 127–139. [[CrossRef](#)]
14. McKnight, M.; Penoyar, P.; Pruett, M.; Palmquist, N.; Jackson, M. New far-infrared laser emissions from optically pumped CH₂DOH, CHD₂OH, and CH₃¹⁸OH. *IEEE J. Quantum Electron.* **2014**, *50*, 42–46. [[CrossRef](#)]
15. Köhler, R.; Tredicucci, A.; Beltram, F.; Beere, H.E.; Rossi, F. Terahertz semiconductor-heterostructure laser. *Nature* **2002**, *417*, 156–159. [[CrossRef](#)]
16. Burford, N.M.; El-Shenawee, M.O. Review of terahertz photoconductive antenna technology. *Opt. Eng.* **2017**, *56*, 10901. [[CrossRef](#)]
17. Yardimci, N.T.; Jarrahi, M. Nanostructure-Enhanced Photoconductive Terahertz Emission and Detection. *Small* **2018**, *14*, 1802437. [[CrossRef](#)]
18. Matsuura, S.; Tani, M.; Sakai, K. Generation of coherent terahertz radiation by photomixing in dipole photoconductive antennas. *Appl. Phys. Lett.* **1997**, *70*, 559–561. [[CrossRef](#)]
19. Aggarwal, R.L.; Lax, B.; Favrot, G. Noncollinear phase matching in GaAs. *Appl. Phys. Lett.* **1973**, *22*, 329–330. [[CrossRef](#)]
20. Moore, W.J.; Holm, R.T. Infrared dielectric constant of gallium arsenide. *J. Appl. Phys.* **1996**, *80*, 6939–6942. [[CrossRef](#)]
21. Skauli, T.; Kuo, P.S.; Vodopyanov, K.L.; Pinguet, T.J.; Levi, O.; Eyres, L.A. Improved dispersion relations for GaAs and applications to nonlinear optics. *J. Appl. Phys.* **2003**, *94*, 6447–6455. [[CrossRef](#)]
22. Lu, Y.; Wang, X.; Miao, L.; Zuo, D.; Cheng, Z. Efficient and widely step-tunable terahertz generation with a dual-wavelength CO₂ laser. *Appl. Phys. B* **2011**, *103*, 387–390. [[CrossRef](#)]
23. Tochitsky, S.Y.; Ralph, J.E.; Sung, C.; Joshi, C. Generation of megawatt-power terahertz pulses by noncollinear difference-frequency mixing in GaAs. *J. Appl. Phys.* **2005**, *98*, 26101. [[CrossRef](#)]
24. Abdullaev, G.B.; Kulevskii, L.A.; Prokhorov, A.M.; Savel'Ev, A.D. GaSe, a new effective material for nonlinear optics. *J. Exp. Theor. Phys. Lett.* **1972**, *16*, 90–95.
25. Vodopyanov, K.L.; Kulevskii, L.A. New dispersion relationships for GaSe in the 0.65–18 μm spectral region. *Opt. Commun.* **1995**, *118*, 375–378. [[CrossRef](#)]
26. Sell, A.; Leitenstorfer, A.; Huber, R. Phase-locked generation and field-resolved detection of widely tunable terahertz pulses with amplitudes exceeding 100 MV/cm. *Opt. Lett.* **2008**, *33*, 2767–2769. [[CrossRef](#)]
27. Jiang, Y.; Ding, Y.J. Efficient terahertz generation from two collinearly propagating CO₂ laser pulses. *Appl. Phys. Lett.* **2007**, *91*, 091108. [[CrossRef](#)]
28. Zhao, P.; Ragam, S.; Ding, Y.J.; Zotova, I.B. Compact and portable terahertz source by mixing two frequencies generated simultaneously by a single solid-state laser. *Opt. Lett.* **2010**, *35*, 3979–3981. [[CrossRef](#)] [[PubMed](#)]
29. Zhao, P.; Ragam, S.; Ding, Y.J.; Zotova, I.B. Investigation of terahertz generation from passively Q-switched dual-frequency laser pulses. *Opt. Lett.* **2011**, *36*, 4818–4820. [[CrossRef](#)] [[PubMed](#)]
30. Liu, Y.; Zhong, K.; Mei, J.L.; Wang, M.R.; Guo, S.B.; Liu, C.; Xu, D.G.; Shi, W.; Yao, J.Q. Compact and flexible dual-wavelength laser generation in coaxial diode-end-pumped configuration. *IEEE Photonics J.* **2017**, *9*, 1–10. [[CrossRef](#)]
31. Zhong, K.; Yao, J.Q.; Xu, D.G.; Zhuo, W.; Li, Z.Y.; Zhang, H.; Zhang, H.Y.; Wang, P. Enhancement of terahertz wave difference frequency generation based on a compact walk-off compensated KTP OPO. *Opt. Commun.* **2010**, *283*, 3520–3524. [[CrossRef](#)]
32. Mei, J.L.; Zhong, K.; Wang, M.R.; Liu, Y.; Xu, D.G.; Shi, W.; Wang, Y.Y.; Yao, J.Q.; Norwood, R.A.; Peyghambarian, N. Widely-tunable high-repetition-rate terahertz generation in GaSe with a compact dual-wavelength KTP OPO around 2 μm. *Opt. Express* **2016**, *24*, 23368–23375. [[CrossRef](#)]

33. Mei, J.L.; Zhong, K.; Wang, M.R.; Liu, Y.; Xu, D.G.; Shi, W.; Wang, Y.Y.; Yao, J.Q.; Liang, W.G. Widely Tunable High-Repetition-Rate Terahertz Generation Based on an Efficient Doubly Resonant Type-II PPLN OPO. *IEEE Photonics J.* **2016**, *8*, 5502107. [[CrossRef](#)]
34. Liu, P.X.; Xu, D.G.; Li, J.Q.; Yan, C.; Li, Z.Y.; Wang, Y.Y.; Yao, J.Q. Monochromatic Cherenkov THz Source Pumped by a Singly Resonant Optical Parametric Oscillator. *IEEE Photonics Technol. Lett.* **2014**, *26*, 494–496. [[CrossRef](#)]
35. Bhar, G.C.; Samanta, L.K.; Ghosh, D.K.; Das, S. Tunable parametric ZnGeP₂ crystal oscillator. *Sov. J. Quantum Electron.* **1987**, *17*, 860. [[CrossRef](#)]
36. Kumbhakar, P.; Kobayashi, T.; Bhar, G.C. Sellmeier dispersion for phase-matched terahertz generation in ZnGeP₂. *Appl. Opt.* **2004**, *43*, 3324–3328. [[CrossRef](#)]
37. Shi, W.; Ding, Y.J.; Schunemann, P.G. Coherent terahertz waves based on difference-frequency generation in an annealed zinc-germanium phosphide crystal: Improvements on tuning ranges and peak powers. *Opt. Commun.* **2004**, *233*, 183–189. [[CrossRef](#)]
38. Creeden, D.; McCarthy, J.C.; Ketteridge, P.A.; Southward, T.; Schunemann, P.G.; Komiak, J.J.; Dove, W.; Chicklis, E.P. Compact fiber-pumped terahertz source based on difference frequency mixing in ZGP. *IEEE J. Sel. Top. Quant. Electron.* **2007**, *13*, 732–737. [[CrossRef](#)]
39. Zhao, P.; Ragam, S.; Ding, Y.J.; Zotova, I.B.; Meissner, H. Singly resonant optical parametric oscillator based on adhesive-free-bonded periodically inverted KTiOPO₄ plates: Terahertz generation by mixing a pair of idler waves. *Opt. Lett.* **2012**, *37*, 1283–1285. [[CrossRef](#)]
40. Brenier, A. THz generation from DFG in a noncollinear phase-matched GaP crystal pumped with a compact diode-pumped two-frequency LiYF₄:Nd laser. *Appl. Phys. B* **2018**, *124*, 194. [[CrossRef](#)]
41. Tanabe, T.; Suto, K.; Nishizawa, J.; Kimura, T.; Saito, K. Frequency-tunable high-power terahertz wave generation from GaP. *J. Appl. Phys.* **2003**, *93*, 4610–4615. [[CrossRef](#)]
42. Tanabe, T.; Suto, K.; Nishizawa, J.; Kimura, T.; Saito, K. Tunable terahertz wave generation in the 3- to 7-THz region from GaP. *Appl. Phys. Lett.* **2003**, *83*, 237–239. [[CrossRef](#)]
43. Tanabe, T.; Suto, K.; Nishizawa, J.; Saito, K.; Kimura, T. Frequency-tunable terahertz wave generation via excitation of phonon-polaritons in GaP. *J. Phys. D Appl. Phys.* **2003**, *36*, 953–957. [[CrossRef](#)]
44. Dantzig, N.; Planken, P.; Bakker, H.J. Far-infrared second-harmonic generation and pulse characterization with the organic salt DAST. *Opt. Lett.* **1998**, *23*, 466–468. [[CrossRef](#)]
45. Kawase, K.; Mizuno, M.; Sohma, S.; Takahashi, H.; Taniuchi, T.; Urata, Y.; Wada, S.; Tashiro, H.; Ito, H. Difference-frequency terahertz-wave generation from 4-dimethylamino-N-methyl-4-stilbazolium-tosylate by use of an electronically tuned Ti: Sapphire laser. *Opt. Lett.* **1999**, *24*, 1065–1067. [[CrossRef](#)]
46. Taniuchi, T.; Okada, S.; Nakanishi, H. Widely tunable terahertz-wave generation in an organic crystal and its spectroscopic application. *J. Appl. Phys.* **2004**, *95*, 5984–5988. [[CrossRef](#)]
47. Ito, H.; Suizu, K.; Yamashita, T.; Nawahara, A.; Sato, T. Random frequency accessible broad tunable terahertz-wave source using phase-matched 4-dimethylamino-N-methyl-4-stilbazolium tosylate crystal. *Jpn. J. Appl. Phys.* **2007**, *46*, 7321. [[CrossRef](#)]
48. Shibuya, T.; Akiba, T.; Suizu, K.; Uchida, H.; Otani, C.; Kawase, K. Terahertz-wave generation using a 4-dimethylamino-N-methyl-4-stilbazolium tosylate crystal under intra-cavity conditions. *Appl. Phys. Express* **2008**, *1*, 42002. [[CrossRef](#)]
49. Tang, M.; Minamide, H.; Wang, Y.Y.; Notake, T.; Ohno, S.; Ito, H. Tunable terahertz-wave generation from DAST crystal pumped by a monolithic dual-wavelength fiber laser. *Opt. Express* **2011**, *19*, 779–786. [[CrossRef](#)]
50. Notake, T.; Nawata, K.; Kawamata, H.; Matsukawa, T.; Qi, F.; Minamide, H. Development of an ultra-widely tunable DFG-THz source with switching between organic nonlinear crystals pumped with a dual-wavelength BBO optical parametric oscillator. *Opt. Express* **2012**, *20*, 25850–25857. [[CrossRef](#)]
51. Dolasinski, B.; Powers, P.E.; Haus, J.W.; Cooney, A. Tunable narrow band difference frequency THz wave generation in DAST via dual seed PPLN OPG. *Opt. Express* **2015**, *23*, 3669–3680. [[CrossRef](#)] [[PubMed](#)]
52. Tokizane, Y.; Nawata, K.; Han, Z.; Koyama, M.; Notake, T.; Takida, Y.; Minamide, H. Tunable terahertz waves from 4-dimethylamino-N'-methyl-4'-stibazolium tosylate pumped with dual-wavelength injection-seeded optical parametric generation. *Appl. Phys. Express* **2017**, *10*, 22101. [[CrossRef](#)]
53. Zhong, K.; Mei, J.L.; Wang, M.R.; Liu, P.X.; Xu, D.G.; Wang, Y.Y.; Shi, W.; Yao, J.Q.; Teng, B.; Xiao, Y. Compact high-repetition-rate monochromatic terahertz source based on difference frequency generation from a dual-wavelength Nd:YAG laser and DAST crystal. *J. Infrared Milli. Terahertz Waves* **2017**, *38*, 87–95. [[CrossRef](#)]
54. Uchida, H.; Ochiai, H.; Suizu, K.; Shibuya, T.; Kawase, K. Improving the Laser-Induced-Damage Tolerance Characteristics of 4-Dimethylamino-N-methyl-4-stilbazoliumtosylate Crystals for THz Wave Generation by Annealing. *Jpn. J. Appl. Phys.* **2012**, *51*, 22601. [[CrossRef](#)]
55. Liu, P.; Feng, Q.; Pang, Z.; Li, W.; Lai, Z. Competition between two parametric processes in a pump source of terahertz-wave difference frequency generation. *J. Phys. D Appl. Phys.* **2018**, *51*, 395102. [[CrossRef](#)]
56. He, Y.Y.; Wang, Y.Y.; Xu, D.G.; Nie, M.T.; Yan, C.; Tang, L.H.; Shi, J.; Feng, J.C.; Yan, D.X.; Liu, H.X.; et al. High-energy and ultra-wideband tunable terahertz source with DAST crystal via difference frequency generation. *Appl. Phys. B-Lasers O.* **2018**, *124*, 16. [[CrossRef](#)]

57. Yang, Z.; Mutter, L.; Stillhart, M.; Ruiz, B.; Aravazhi, S.; Jazbinsek, M.; Schneider, A.; Gramlich, V.; Guenter, P. Large-size bulk and thin-film stilbazolium-salt single crystals for nonlinear optics and THz generation. *Adv. Funct. Mater.* **2007**, *17*, 2018–2023. [[CrossRef](#)]
58. Matsukawa, T.; Yoshimura, M.; Takahashi, Y.; Takemoto, Y.; Takeya, K.; Kawayama, I.; Okada, S.; Tonouchi, M.; Kitaoka, Y.; Mori, Y.; et al. Bulk Crystal Growth of Stilbazolium Derivatives for Terahertz Waves Generation. *Jpn. J. Appl. Phys.* **2010**, *49*, 75502. [[CrossRef](#)]
59. Matsukawa, T.; Notake, T.; Nawata, K.; Inada, S.; Okada, S.; Minamide, H. Terahertz-wave generation from 4-dimethylamino-N'-methyl-4'-stilbazolium p-bromobenzenesulfonate crystal: Effect of halogen substitution in a counter benzenesulfonate of stilbazolium derivatives. *Opt. Mater.* **2014**, *36*, 1995–1999. [[CrossRef](#)]
60. Liu, P.X.; Xu, D.G.; Li, Y.; Zhang, X.Y.; Wang, Y.Y.; Yao, J.Q.; Wu, Y.C. Widely tunable and monochromatic terahertz difference frequency generation with organic crystal DSTMS. *Europhys. Lett.* **2014**, *106*, 60001. [[CrossRef](#)]
61. Walther, M.; Jensby, K.; Keiding, S.R.; Takahashi, H.; Ito, H. Far-infrared properties of DAST. *Opt. Lett.* **2000**, *25*, 911–913. [[CrossRef](#)]
62. Brunner, F.; Kwon, O.P.; Kwon, S.J.; Jazbinsek, M.; Günter, P. A hydrogen-bonded organic nonlinear optical crystal for high-efficiency terahertz generation and detection. *Opt. Express* **2008**, *16*, 16496–16508. [[CrossRef](#)]
63. Hashimoto, H.; Okada, Y.; Fujimura, H.; Morioka, M.; Sugihara, O.; Okamoto, N.; Matsushima, R.M.R. Second-Harmonic Generation from Single Crystals of N-Substituted 4-Nitroanilines. *Jpn. J. Appl. Phys.* **1997**, *36*, 6754–6760. [[CrossRef](#)]
64. Choi, E.Y.; Jazbinsek, M.; Kwon, O.P. Control of Nucleation of Organic Electrooptic Phenolic Polyene Crystals by Highly Polar Liquid Additive. *Cryst. Growth Des.* **2012**, *12*, 495–498. [[CrossRef](#)]
65. Kim, P.J.; Jeong, J.H.; Jazbinsek, M.; Choi, S.B.; Baek, I.H.; Kim, J.T.; Rotermund, F.; Yun, H.; Lee, Y.S.; Kwon, O.P. Highly Efficient Organic THz Generator Pumped at Near-Infrared: Quinolinium Single Crystals. *Adv. Funct. Mater.* **2012**, *22*, 200–209. [[CrossRef](#)]
66. Jeong, J.H.; Kang, B.J.; Kim, J.S.; Jazbinsek, M.; Lee, S.H.; Lee, S.C.; Baek, I.H.; Kim, J.; Lee, Y.S.; Kim, J.T.; et al. High-power Broadband Organic THz Generator. *Sci. Rep.* **2013**, *3*, 3320. [[CrossRef](#)]
67. Myers, L.E.; Eckardt, R.C.; Fejer, M.M.; Byer, R.L.; Pierce, J.W. Quasi-phase-matched optical parametric oscillators in bulk periodically poled LiNbO₃. *J. Opt. Soc. Am. B* **1995**, *12*, 2102–2116. [[CrossRef](#)]
68. Gordon, L.; Woods, G.L.; Eckardt, R.C.; Route, R.R.; Feigelson, R.S.; Fejer, M.M.; Byer, R. Diffusion-bonded stacked GaAs for quasi phase-matched second-harmonic generation of a carbon dioxide laser. *Electron. Lett.* **1993**, *29*, 1942–1944. [[CrossRef](#)]
69. Eyres, L.A.; Turreau, P.J.; Pinguet, T.J.; Ebert, C.B.; Harris, J.S.; Fejer, M.M.; Becouarn, L.; Gerard, B.; Lallier, E. All-epitaxial fabrication of thick, orientation-patterned GaAs films for nonlinear optical frequency conversion. *Appl. Phys. Lett.* **2001**, *79*, 904–906. [[CrossRef](#)]
70. Sasaki, Y.; Yuri, A.; Kawase, K.; Ito, H. Terahertz-wave surface-emitted difference frequency generation in slant-stripe-type periodically poled LiNbO₃ crystal. *Appl. Phys. Lett.* **2002**, *81*, 3323–3325. [[CrossRef](#)]
71. Sasaki, Y.; Avetisyan, Y.; Yokoyama, H.; Ito, H. Surface-emitted terahertz-wave difference-frequency generation in two-dimensional periodically poled lithium niobate. *Opt. Lett.* **2005**, *30*, 2927–2929. [[CrossRef](#)]
72. Scheller, M.; Yarborough, J.M.; Moloney, J.V.; Fallahi, M.; Koch, M.; Koch, S.W. Room temperature continuous wave milliwatt terahertz source. *Opt. Express* **2010**, *18*, 27112–27117. [[CrossRef](#)]
73. Wang, T.D.; Lin, S.T.; Lin, Y.Y.; Chiang, A.C.; Huang, Y.C. Forward and backward terahertz-wave difference-frequency generations from periodically poled lithium niobate. *Opt. Express* **2008**, *16*, 6471–6478. [[CrossRef](#)]
74. Vodopyanov, K.L. Optical THz-wave generation with periodically inverted GaAs. *Laser Photonics Rev.* **2008**, *2*, 11–25. [[CrossRef](#)]
75. Zhao, P.; Ragam, S.; Ding, Y.J.; Zotova, I.B. Terahertz intracavity generation from output coupler consisting of stacked GaP plates. *Appl. Phys. Lett.* **2012**, *101*, 21107. [[CrossRef](#)]
76. Petersen, E.B.; Shi, W.; Chavez-Pirson, A.; Peyghambarian, N.; Cooney, A.T. Efficient parametric terahertz generation in quasi-phase-matched GaP through cavity enhanced difference-frequency generation. *Appl. Phys. Lett.* **2011**, *98*, 121119. [[CrossRef](#)]
77. Jiang, Y.; Li, D.; Ding, Y.J.; Zotova, I.B. Terahertz generation based on parametric conversion: From saturation of conversion efficiency to back conversion. *Opt. Lett.* **2011**, *36*, 1608–1610. [[CrossRef](#)]
78. Vodopyanov, K.L.; Hurlbut, W.C.; Kozlov, V.G. Photonic THz generation in GaAs via resonantly enhanced intracavity multispectral mixing. *Appl. Phys. Lett.* **2011**, *99*, 41104. [[CrossRef](#)]
79. Schaar, J.E.; Vodopyanov, K.L.; Fejer, M.M. Intracavity terahertz-wave generation in a synchronously pumped optical parametric oscillator using quasi-phase-matched GaAs. *Opt. Lett.* **2007**, *32*, 1284–1286. [[CrossRef](#)]
80. Kiessling, J.; Breunig, I.; Schunemann, P.G.; Buse, K.; Vodopyanov, K.L. High power and spectral purity continuous-wave photonic THz source tunable from 1 to 4.5 THz for nonlinear molecular spectroscopy. *New J. Phys.* **2013**, *15*, 105014. [[CrossRef](#)]
81. Tyszkiewicz, C. Homogeneous sensitivity of sol-gel derived planar waveguide structures-theoretical analysis. *Opt. Appl.* **2012**, *42*, 555–569.
82. Thompson, D.E.; Coleman, P.D. Step-tunable far infrared radiation by phase matched mixing in planar-dielectric waveguides. *IEEE Trans. Microw. Theory Tech.* **1974**, *22*, 995–1000. [[CrossRef](#)]
83. Marandi, A.; Darcie, T.E.; So, P.P. Design of a continuous-wave tunable terahertz source using waveguide-phase-matched GaAs. *Opt. Express* **2008**, *16*, 10427–10433. [[CrossRef](#)] [[PubMed](#)]
84. Zangeneh, H.R.; Asadnia Fard Jahromi, M.; Asadnia Fard Jahromi, M. Design of a terahertz source using a nano-slot of GaAs. *J. Opt. UK* **2014**, *43*, 173–176. [[CrossRef](#)]

85. Vodopyanov, K.L.; Avetisyan, Y.H. Optical terahertz wave generation in a planar GaAs waveguide. *Opt. Lett.* **2008**, *33*, 2314–2316. [[CrossRef](#)] [[PubMed](#)]
86. Nishizawa, J.I.; Suto, K.; Tanabe, T.; Saito, K.; Kimura, T.; Oyama, Y. THz generation from GaP rod-type waveguides. *IEEE Photonics Technol. Lett.* **2007**, *19*, 143–145. [[CrossRef](#)]
87. Saito, K.; Tanabe, T.; Oyama, Y. Elliptically polarized THz-wave generation from GaP-THz planar waveguide via collinear phase-matched difference frequency mixing. *Opt. Express* **2012**, *20*, 26082–26088. [[CrossRef](#)]
88. Saito, K.; Tanabe, T.; Oyama, Y. Widely tunable terahertz-wave generation from planar GaP waveguides via difference frequency generation under collinear phase-matching condition. *Jpn. J. Appl. Phys.* **2014**, *53*, 102203. [[CrossRef](#)]
89. De Regis, M.; Bartalini, S.; Ravaro, M.; Calonico, D.; De Natale, P.; Consolino, L. Room-Temperature Continuous-Wave Frequency-Referenced Spectrometer up to 7.5 THz. *Phys. Rev. Appl.* **2018**, *10*, 064041. [[CrossRef](#)]
90. Suizu, K.; Suzuki, Y.; Sasaki, Y.; Ito, H.; Avetisyan, Y. Surface-emitted terahertz-wave generation by ridged periodically poled lithium niobate and enhancement by mixing of two terahertz waves. *Opt. Lett.* **2006**, *31*, 957–959. [[CrossRef](#)]
91. Saito, K.; Tanabe, T.; Oyama, Y. THz-wave generation via difference frequency mixing in strained silicon based waveguide utilizing its second order susceptibility $\chi(2)$. *Opt. Express* **2014**, *22*, 16660–16668. [[CrossRef](#)]
92. Schulz, K.M.; Rusche, A.G.; Petrov, A.Y.; Eich, M. Integrated nonlinear waveguide optics for high-efficiency and wideband-tunable generation of THz radiation. *ACS Photonics* **2018**, *5*, 3779–3787. [[CrossRef](#)]
93. Ding, Y.J. Terahertz parametric converters by use of novel metallicdielectric hybrid waveguides. *J. Opt. Soc. Am. B* **2006**, *23*, 1354–1359. [[CrossRef](#)]
94. Liu, P.X.; Shi, W.; Xu, D.G.; Zhang, X.Z.; Yao, J.Q.; Norwood, R.A.; Peyghambarian, N. High-power high-brightness terahertz source based on nonlinear optical crystal fiber. *IEEE J. Sel. Top. Quantum Electron.* **2016**, *22*, 360–364. [[CrossRef](#)]
95. Cherchi, M.; Taormina, A.; Busacca, A.C.; Oliveri, R.L.; Leone, C. Exploiting the optical quadratic nonlinearity of zinc-blende semiconductors for guidedwave terahertz generation: A material comparison. *IEEE J. Quantum Electron.* **2010**, *46*, 368–376. [[CrossRef](#)]
96. Mei, J.L.; Zhong, K.; Xu, J.M.; Xu, D.G.; Shi, W.; Yao, J.Q. Efficient Terahertz Generation Via GaAs Hybrid Ridge Waveguides. *IEEE Photonics Technol. Lett.* **2019**, *31*, 1666–1669. [[CrossRef](#)]
97. Lu, X.; Ota, H.; Kumagai, N.; Minami, Y.; Kitada, T.; Isu, T. Two-color surface-emitting lasers by a GaAs-based coupled multilayer cavity structure for coherent terahertz light sources. *J. Cryst. Growth* **2017**, *477*, 249–252. [[CrossRef](#)]
98. Kitada, T.; Katoh, S.; Takimoto, T.; Nakagawa, Y.; Morita, K.; Isu, T. Terahertz emission from a GaAs/AlAs coupled multilayer cavity with nonlinear optical susceptibility inversion. *Appl. Phys. Lett.* **2013**, *102*, 251118. [[CrossRef](#)]
99. Kitada, T.; Tanaka, F.; Takahashi, T.; Morita, K.; Isu, T. GaAs/AlAs coupled multilayer cavity structures for terahertz emission devices. *Appl. Phys. Lett.* **2009**, *95*, 111106. [[CrossRef](#)]
100. Ashkin, A.; Boyd, G.; Dziedzic, J. Resonant optical second harmonic generation and mixing. *IEEE J. Quantum Electron.* **1966**, *2*, 109–124. [[CrossRef](#)]
101. Kozlovsky, W.J.; Nabors, C.D.; Byer, R.L. Efficient second harmonic generation of a diode-laser-pumped CW Nd:YAG laser using monolithic MgO:LiNbO₃ external resonant cavities. *IEEE J. Quantum Electron.* **1988**, *24*, 913–919. [[CrossRef](#)]
102. Tanaka, R.; Matsuzawa, T.; Yokota, H.; Suzuki, T.; Fujii, Y.; Mio, A.; Katsuragawa, M. Stable confinement of nanosecond laser pulse in an enhancement cavity. *Opt. Express* **2008**, *16*, 18667–18674. [[CrossRef](#)]
103. Theuer, M.; Molter, D.; Maki, K.; Otani, C.; L’huillier, J.A.; Beigang, R. Terahertz generation in an actively controlled femtosecond enhancement cavity. *Appl. Phys. Lett.* **2008**, *93*, 41119. [[CrossRef](#)]
104. Petersen, E.B.; Shi, W.; Nguyen, D.T.; Yao, Z.; Zong, J.; Chavez-Pirson, A.; Peyghambarian, N. Enhanced terahertz source based on external cavity difference-frequency generation using monolithic single-frequency pulsed fiber lasers. *Opt. Lett.* **2010**, *35*, 2170–2172. [[CrossRef](#)]
105. Paul, J.R.; Scheller, M.; Laurain, A.; Young, A.; Koch, S.W.; Moloney, J. Narrow linewidth single frequency terahertz source based on difference frequency generation of vertical-external-cavity source-emitting lasers in an external resonance cavity. *Opt. Lett.* **2013**, *38*, 3654–3657. [[CrossRef](#)]
106. Cronin-Golomb, M. Cascaded nonlinear difference-frequency generation of enhanced terahertz wave production. *Opt. Lett.* **2004**, *29*, 2046–2048. [[CrossRef](#)]
107. Schaar, J.E.; Vodopyanov, K.L.; Kuo, P.S.; Fejer, M.M.; Yu, X.J.; Lin, A.; Harris, J.S.; Bliss, B.; Lynch, C.; Kozlov, V.G.; et al. Terahertz sources based on intracavity parametric down-conversion in quasi-phase-matched gallium arsenide. *IEEE J. Sel. Top. Quantum Electron.* **2008**, *14*, 354–362. [[CrossRef](#)]
108. Zhong, K.; Yao, J.Q.; Xu, D.G.; Zhang, H.Y.; Wang, P. Theoretical research on cascaded difference frequency generation of terahertz radiation (in Chinese). *Acta. Phys. Sin.* **2011**, *60*, 34210. [[CrossRef](#)]
109. Hu, C.F.; Zhong, K.; Mei, J.L.; Wang, M.R.; Guo, S.B.; Xu, W.Z.; Liu, P.X.; Xu, D.G.; Wang, Y.Y.; Yao, J.Q. Theoretical analysis of terahertz generation in periodically inverted nonlinear crystals based on cascaded difference frequency generation process. *Mod. Phys. Lett. B* **2015**, *29*, 1450263. [[CrossRef](#)]
110. Ravi, K.; Hemmer, M.; Cirmi, G.; Reichert, F.; Schimpf, D.N.; Mücke, O.D.; Kärtner, F.X. Cascaded parametric amplification for highly efficient terahertz generation. *Opt. Lett.* **2016**, *41*, 3806–3809. [[CrossRef](#)]